Modified Bovine Milk Exosomes for Doxorubicin Delivery to Triple-Negative Breast Cancer Cells

Jessica Pullan[1], Kaitlin Dailey[2], Sangeeta Bhallamudi[1], Li Feng[1], Lina Alhalhooly[3], Jamie Froberg[3], Jenna Osborn[4], Kausik Sarkar[4], Todd Molden[5], Venkatachalem Sathish[1], Yongki Choi[3], Amanda Brooks[6], Sanku Mallik*[1]

Author Affiliations:
[1] Department of Pharmaceutical Sciences, North Dakota State University, Fargo, North Dakota 58105 USA.
[2] Cell and Molecular Biology Program, North Dakota State University, Fargo, North Dakota 58105 USA.
[3] Department of Physics, North Dakota State University, Fargo, North Dakota 58105 USA.
[4] Department of Mechanical and Aerospace Engineering, George Washington University, Washington, District of Columbia 20052 USA.
[5] Department of Animal Science, North Dakota State University, Fargo, North Dakota 58105 USA
[6] Office of Research and Scholarly Activity, Rocky Vista University, Ivins, Utah 84738 USA.

KEYWORDS. Exosomes, doxorubicin, hypoxia-responsive, iRGD, targeted-drug delivery

ABSTRACT: Biological nanoparticles, such as exosomes, offer an approach to drug delivery due to their innate ability to transport biomolecules. Exosomes are derived from cells and an integral component of cellular communication. However, the cellular cargo of human exosomes could negatively impact their use as a safe drug carrier. Additionally, exosomes have the intrinsic yet enigmatic, targeting characteristics of complex cellular communication. Hence, harnessing the natural transport abilities of exosomes for drug delivery requires predictably targeting these biological nanoparticles. This manuscript describes the use of two chemical modifications, incorporating a neuropilin receptor agonist peptide (iRGD) and a hypoxia-responsive lipid for targeting and release of an encapsulated drug from bovine milk exosomes to triple-negative breast cancer cells. Triple-negative breast cancer is a very aggressive and deadly form of malignancy with limited treatment options. Incorporation of both the iRGD peptide and hypoxia-responsive lipid into the lipid bilayer of bovine milk exosomes and encapsulation of the anticancer drug, doxorubicin, created the peptide targeted, hypoxia-responsive bovine milk exosomes, iDHRX. Initial studies confirmed the presence of iRGD peptide and the exosomes' ability to target the $\alpha_v\beta_3$ integrin, overexpressed on triple-negative breast cancer cells' surface. These modified exosomes were stable under normoxic conditions but fragmented in the reducing microenvironment created by 10 mM glutathione. *In vitro* cellular internalization studies in monolayer and three-dimensional (3D) spheroids of triple-negative breast cancer cells confirmed the cell-killing ability of iDHRX. Cell viability of 50% was reached at 10 μM iDHRX in the 3D spheroid models using four different triple-negative breast cancer cell lines. Overall, the tumor penetrating, hypoxia-responsive exosomes encapsulating doxorubicin would be effective in reducing triple-negative breast cancer cells' survival.

1. Introduction:

With a 5-year overall survival rate of 90%, breast cancer appears to be a problem of the past. [1] However, triple-negative breast cancer (TNBC) has a 77% 5-year mortality rate, regardless of the stage.[2] TNBC cells lack estrogen receptors, progesterone receptors, and human epidermal growth factor receptor 2 (HER2) receptors, limiting current treatment strategies' effectiveness.[3,4] Out of the over 1,151,000 patients in the U.S. diagnosed annually with breast cancer, 10-15% will be TNBC.[2] Further compromising the efficacy of treatment, TNBC is often characterized by its aggressive, metastatic nature and frequent reoccurrence.[5,6] Metastatic cells often have genetic abnormalities, leading to refractory cancer.[7,8] Finding a strategy that is either unaffected by these changes or can account for them is necessary to prevent metastatic sites from growing unabated. One such approach is targeting the unique aspects of the tumor microenvironment.

Solid tumors of TNBC have a unique cellular microenvironment that drug delivery systems could exploit. At a diameter greater than 100-180 μm, a solid tumor forms a dense cellular environment that continues to evolve as the tumor grows.[9] These local environment changes lead to unusual fluid flow within the tumor, lack of sufficient oxygen and nutrient exchange, and compromised therapeutic efficacy of anticancer drugs beyond the diffusion limit of the normal tissue margins.[10,11] Some of the unique characteristics of the tumor microenvironment include densely-packed cells, abnormal angiogenesis, increased acidity, acute hypoxia (< 1% oxygen), and upregulation of several markers, such as hypoxia-inducible factors (HIFs), carbonic anhydrases, neuropilin-1 receptor, $\alpha_v\beta_3$ integrin, etc.[12–22] Hypoxia[23] has been utilized with some success in drug delivery;[24,25] however, penetration of the carriers into solid tumors to reach the hypoxic niches is still a challenge. Combining a hypoxia sensing strategy to release the drug payload only to the previously inaccessible "inter-tumor" with an integrated tumor penetrating peptide, which targets altered biomolecule expression, may provide a therapeutic drug level to the deepest recesses of the tumor while protecting healthy host tissue. Such an elegant design is possible by using exosomes.

This biologically-driven approach will lead to decreased off-target effects and more effective drug delivery. [26–29]

Despite important pre-clinical and clinical data and a limited number of FDA-approved nanoparticle-based products, late-stage clinical trial failures continue to plague the field.[29] Some of these issues include toxicity and immune clearance.[29] Exosomes may circumvent these hurdles due to their biological origin.[30] Exosomes are nanosized (30-150 nm), extracellular vesicles secreted from cells (Figure 1)[30] for cellular communication.[31,32] The innate ability to transport biomolecules for communication makes exosomes uniquely suited as drug carriers. Exosomes provide many drug delivery options and diagnostics and can be isolated from multiple bodily fluids across species, including bovine milk.[30] However, their cargo could communicate an unintended, even metastatic[33,34] message, posing a significant barrier for clinical translation. In contrast, the non-human exosomes are safer and more readily available.[33,34] Raw bovine milk is an attractive source of exosomes due to availability, low immunogenicity, low aggregation and lack of human molecular cargo, and consequently, without unintended cellular communications.[30,35,36]

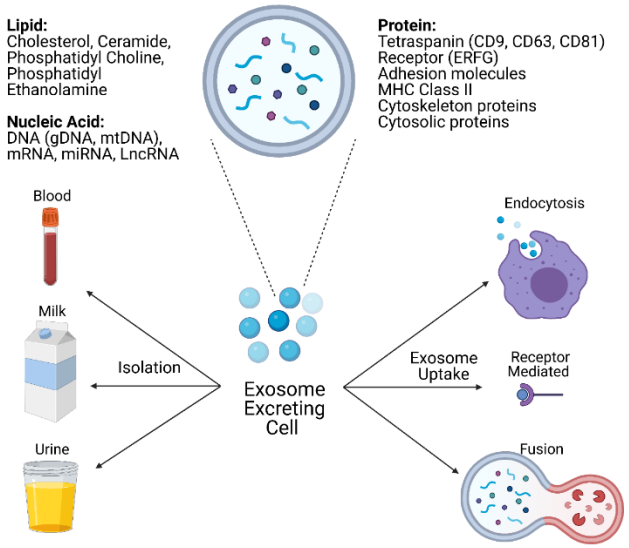

Figure 1. Exosome secretion, structure, and uptake. Cell-secreted exosomes transport biomolecules throughout the body to receptor cells, where uptake occurs through three main mechanisms: fusion, receptor-ligand interaction, endocytosis. Exosome structures include lipids, proteins, and nucleic acids from secreting cells and vary based on cellular origin.

While bovine milk exosomes may be safer and readily available, their development as a drug delivery system is hindered by the inability of exosomes (regardless of their source) to target and penetrate a tumor and deliver the drug payload. In the current study, bovine milk exosomes were chemically modified to target the altered microenvironment of TNBC, penetrate, and deliver the encapsulated chemotherapeutic drug to three-dimensional (3D) tumor spheroids. A hypoxia-responsive lipid and a tumor penetrating peptide were incorporated into the lipid bilayer of the exosomes. The hypoxia-responsive lipid was designed to be reductively cleaved in the hypoxic niches of a solid tumor, allowing for a burst release of the encapsulated drug. We incorporated the reported neuropilin-1 receptor (NRP-1) agonist iRGD peptide on the exosomes for targeting and tumor penetration. The TNBC cells, especially under hypoxia, overexpress NRP-1 and the $\alpha_v\beta_3$ integrin on the surface.[24,26–28,37–44] Hence, the modified bovine milk exosomes with both the hypoxia-responsive lipid and the iRGD tumor targeting and penetrating peptide should result in significant cell death in an *in vitro* 3D spheroid model of TNBC.

2. Materials and Methods:

Exosome isolation:

The procedure for exosome isolation was the same as previously reported.[45] Raw bovine milk was collected from the North Dakota State University Dairy Farm. We observed that the raw milk could be stored at 4 °C for four days without impacting the isolation of exosomes. Sequential centrifugation was used to isolate exosomes. Briefly, raw bovine milk was initially centrifuged for 20 minutes at 3,500 g (VWR Clinical 200 Centrifuge). To remove the white fat deposits collected on the sides of the centrifuge tubes, the milk was passed through a cheesecloth. The milk was collected and placed into a thin wall, Ultra-Clear tubes (Beckman Coulter), and centrifuged at 12,950 g at 4 °C for 30 minutes (Beckman Coulter Optima XPN-80 ultracentrifuge with an S.W. 41 Ti rotor). The milk was removed from the tubes and was again filtered through a cheesecloth to remove fat. The filtered milk was placed in new ultracentrifuge tubes and spun at 98,500 g for 70 minutes at 4 °C. After ultra-centrifugation, three layers were evident in each tube. The middle whey layer was collected, transferred to two new tubes, and centrifuged at 135,030 g for 105 minutes at 4 °C. Subsequently, the supernatant was removed, taking care not to disturb the exosome pellet. The pellet was then resuspended in 1 mL of phosphate buffer saline (PBS) (1X Dulbecco's PBS, pH 7.4, VWR). A 0.2 µm filter was pre-wet using PBS, and the suspended exosomes were passed through the filter into an Eppendorf tube. The first three drops of PBS were discarded, and the remaining filtrate was collected. Notably, exosome recovery was maximized by dividing the PBS exosome suspension between two different syringe filters. Additionally, the exosome filtrate was washed with additional PBS, and the first three drops were collected with the previous exosome filtrate. Dynamic light scattering (DLS) (ZS90, Malvern Panalytical) was performed to determine exosomes' hydrodynamic diameters. The isolated exosomes were stored at –80 °C until used (see Supporting Information, Figure S1 for a detailed exosome isolation scheme).

Exosome counting and size distribution by tunable resistive pulse sensing:

All measurements were performed using qNano Gold (Izon Science) using a nanopore size NP150. The sample size and concentration were calibrated during each measurement using the manufacturer's calibration particles, carboxylated polystyrene beads (CPC100, average diameter: 110 nm, concentration: 1.1 x 10^{13} particles/mL). Exosomes were diluted 100-500 times for optimal counting using two different pressures of 4 and 8 mbar. At least 8 replicates were performed for each sample for each measurement.

Hypoxia responsive lipid synthesis:
We followed a synthetic protocol reported from our laboratory.[24,45] NMR (400 MHz Bruker Avance III HD) and ESI TOF Mass Spectroscopy were used to confirm the hypoxia responsive lipid structure (Figure 2, Supporting Information Figures S4 and S5).

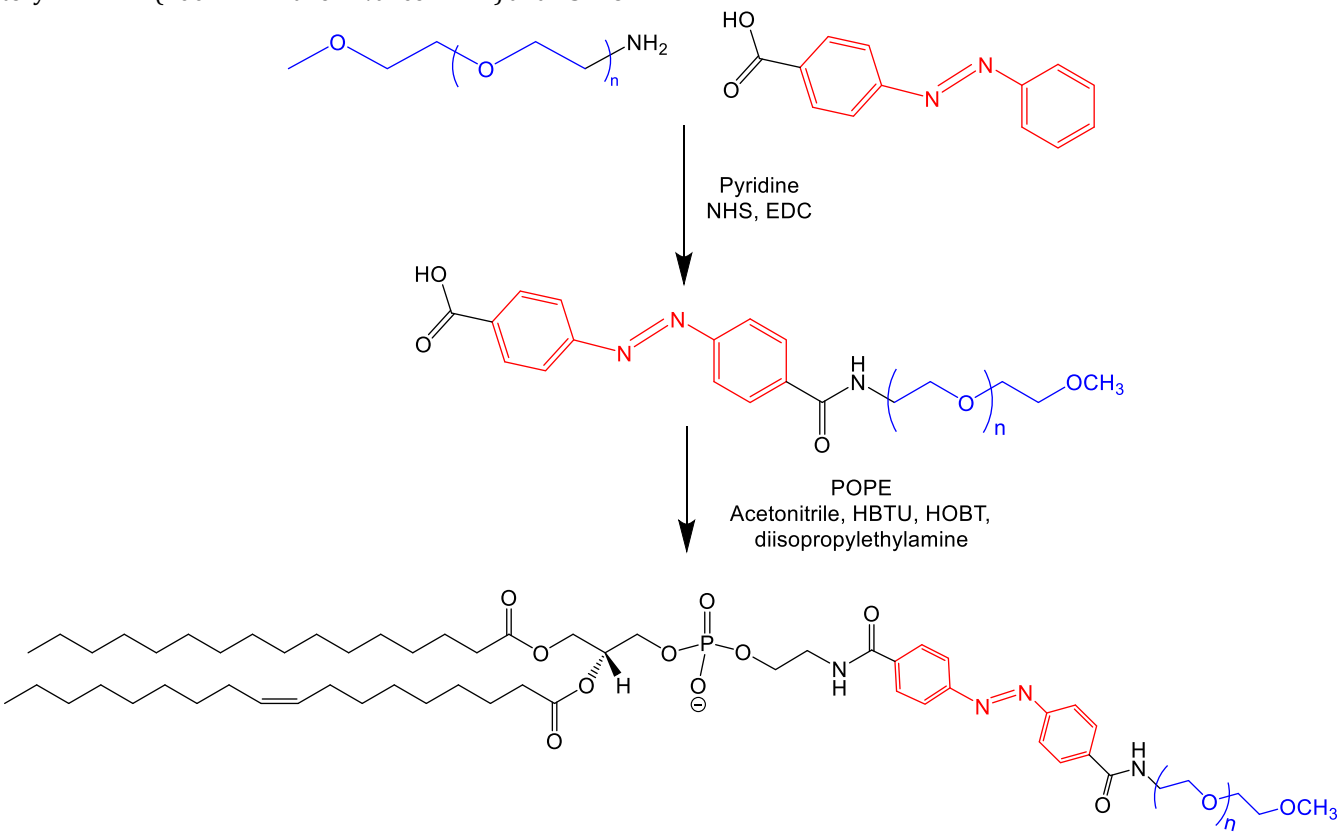

Figure 2. Synthetic scheme of hypoxia-responsive lipid, POPE-Azobenzene-PEG$_{1800}$.

Hypoxia-responsive lipid incorporation into exosomes:
The hypoxia-responsive lipid was incorporated into the exosome bilayer according to our previously reported protocol.[45] Exosomes were removed from the –80 °C freezer and thawed. A 5 mg/mL solution of the hypoxia-responsive lipid in PBS was sonicated for 30 minutes to ensure complete dissolution. Hypoxia responsive lipid (80 µL) and purified exosomes (120 µL) were gently mixed and subsequently incubated at 37 °C for one hour. After incubation, 100 µL PBS was added to create a homogeneous mixture. The liquid was placed into a centrifugal filter (Nanosep Centrifugal Devices; MWCO: 100,000; Pall Corporation) and centrifuged at 9,400 g for 10 minutes to remove any unincorporated lipid. The liquid on top of the filter was used to resuspend any exosomes. All of the liquid (containing the exosomes) was removed, placed in an Eppendorf tube, and stored at –80 °C until use.

Estimation of hypoxia-responsive lipid concentration in exosomes:
The amount of hypoxia-responsive lipid incorporated into the exosomes was estimated based on the presence of the PEG$_{1800}$ using a PEGylated Protein ELISA (Enzo Life Sciences) according to the manufacturer's protocol. A series of dilutions in PBS (1.75 to 225 ng/mL) was performed to establish a standard curve. The optimum mixing ratio of hypoxia-responsive lipid to exosome for efficient incorporation was determined. Initial lipid solutions used include 1 mg/mL and 5 mg/mL, with ratios of lipid solution to exosomes of 1:1, 1:2, 1:4, and 3:4 (by volume).

DSPE-PEG$_{5000}$-iRGD synthesis:
DSPE-PEG$_{5000}$-N$_3$ (NanOCS) was reacted with the alkyne (hexynoic acid) moiety of a synthesized iRGD peptide using click chemistry (1:2 molar ratio peptide to polymer) (Figure 3). The copper complex was prepared by mixing copper(II) sulfate with N,N,N′,N′,N″-pentamethyl diethylenetriamine (PMDETA) for 2 hours. An ascorbic acid solution (1.4 µmol) was prepared in distilled water. The reaction mixture was then stirred for 72 hours at room temperature. Subsequently, the solution was transferred to a 3.5-5 kDa dialysis bag and dialyzed against water for 72 hours to remove PMDETA, ascorbic acid, as well as unreacted iRGD peptide. The product was lyophilized and analyzed by CD spectroscopy (J-815 CD Spectrometer, Jasco) with 64 scans and at 4 °C.

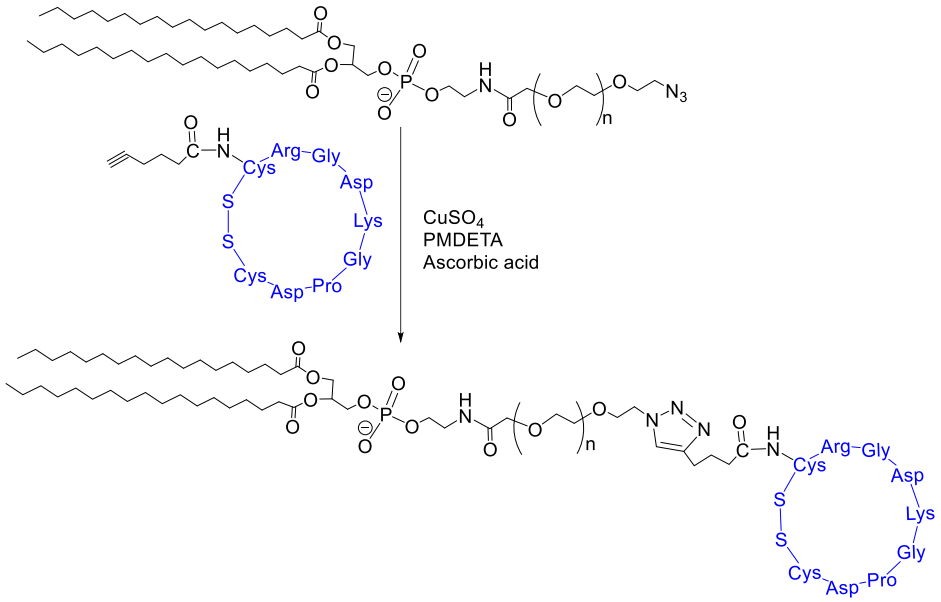

Figure 3. Synthesis of DSPE-PEG$_{5000}$-iRGD.

DSPE-PEG$_{5000}$-iRGD incorporation in exosomes:
Incorporation of DPSE-PEG$_{5000}$-iRGD in the exosomes was performed according to our previously reported protocol.[45] A 5 mg/mL solution of the DPSE-PEG$_{5000}$-iRGD in PBS was prepared and sonicated for 1 hour to ensure complete dissolution. DPSE-PEG$_{5000}$-iRGD solution (80 µL) and hypoxia-responsive exosomes (120 µL) were gently mixed and incubated at 37 °C for one hour. After incubation, 100 µL PBS was added, and the solution was ultrafiltered using a centrifugal filter (Nanosep Centrifugal Devices with 100,000 cut-off membrane, Pall Corporation) at 9,400 g for 10 minutes to remove any unincorporated peptide conjugate. The liquid on top was used to resuspend any exosomes on the filter. The liquid was removed, placed in an Eppendorf tube, and stored at –80 °C until use.

Encapsulation of doxorubicin in exosomes:
Doxorubicin hydrochloride (Advanced ChemBlocks) was encapsulated into either modified or unmodified exosomes using electroporation (40 V, 125 µF, and 750 Ω). After electroporation, exosomes were placed at 37 °C for 1 hour. Hypoxia-responsive, iRGD targeting exosomes (iHRX) were centrifuged at 9,400 g for 10 minutes in a centrifugal filter (Nanosep Centrifugal Devices with 100,000 cut-off membranes, Pall Corporation) to remove the free drug. Encapsulation efficiency was determined by UV-Vis Spectrophotometry (SpectraMax M5, Molecular Devices) for doxorubicin (480 nm).

Atomic Force Microscopy (AFM):
Samples for AFM were prepared by placing 10 µL of each solution (control or exosomes) on silicon substrates (University Wafer) for 10 minutes in a sealed chamber to prevent evaporation at room temperature. The samples were then washed with de-ionized water (Millipore) and dried under nitrogen gas. Imaging measurements were performed using a commercial atomic force microscope (NT-MDT NTEGRA AFM). Samples were imaged under ambient conditions in semi-contact mode using an AFM tip with a resonant frequency of 190 kHz (Budget sensors).

High-Resolution Transmission Electron Microscopy (HRTEM):
A drop of the sample (control or exosome containing) was placed on a 300-mesh formvar-carbon coated copper TEM grid (Electron Microscopy Sciences, Hatfield, Pennsylvania, USA) for 1 minute and wicked off. Phosphotungstic acid 0.1%, pH adjusted to 7-8, was dropped onto the grid, allowed to stand for 2 minutes, and then wicked off. After the grids were dry, images were obtained using a JEOL JEM-2100 LaB_6 transmission electron microscope (JEOL USA, Peabody, Massachusetts) running at 200 kV. Magnification reported is for images at size 3.25 x 4 inches.

Flow Cytometry analysis of CD63 in exosomes:
Freshly isolated bovine milk exosomes were suspended in 500 µL of PBS containing anti-CD63 monoclonal antibody (1:500 dilution, CC25, Invitrogen) and allowed to rock at room temperature for 30 minutes to facilitate interaction. Exosomes were then washed with PBS three times to remove the unbound antibody, centrifuging at 10,000 g for 10 minutes after each wash. Goat anti-mouse IgG antibody in PBS (1:1000 dilution, GtxMu-003-FFITC, ImmunoReagents) was then added and allowed to rock at room temperature for 30 minutes. Subsequently, the secondary antibody was removed, and the exosomes were again washed three times with PBS to remove the unbound secondary antibody. Exosomes were resuspended in 500 µL of PBS, and flow cytometry was performed using BD Accuri C6 Flow Cytometer. Twenty thousand events were captured for each sample (Supporting Information, Figure S7).

Incubation of HRX with glutathione:
A stock solution (50 mM) of glutathione was prepared in phosphate-buffered saline (PBS, Corning). Four glutathione (reduced free acid, EMD Millipore) solutions were prepared: 10 mM, 5 mM, 1 mM, and 50 µM. Concentrations were chosen to mimic the reducing environment within a tumor and that commonly found in the blood.[46,47] A 10% dilution of hypoxia-responsive exosomes was added to each of the glutathione solutions. Dynamic light scattering (DLS)

was used to monitor exosomes' size every 10 minutes for 2 hours. AFM imaging was also performed after 10 minutes and 2 hours of incubation, as described above.

Adhesion assay with $\alpha_v\beta_3$ integrin:
To monitor exosomes' interactions, DSPE-PEG_{5000}-FITC (NANOCS) was incorporated into the exosomes' lipid bilayer through the same method as described for DSPE-PEG_{5000}-iRGD. Groups tested for this study included integrin-coated coverslips treated with PBS (control), FITC tagged exosomes (control), and FITC labeled iHRX. Circular borosilicate glass covers slips (Fisher Scientific) was corona (air plasma) (Enercon Compak 2000 Corona Treater Model LM4045-06) treated with the wand passing over both sides of the coverslip four times. Treated coverslips were then placed in 6-well plates (Celltreat). Untreated coverslips were used as a control. After corona treatment, 100 µL of 10 µg/mL $\alpha_v\beta_3$ integrin (carrier-free, human recombinant protein, R&D Systems) or the carrier solution (PBS) was added to the coverslip and left at 4 °C to evaporate to dryness. After 48 hours of drying, 100 µL of treatment (buffer or exosomes) was added to the integrin-treated slides. Coverslips were then placed at 4 °C, and the iRGD peptide was allowed to interact with the integrin for 48 hours while the water on the slides was evaporated to dryness. Slides were then washed with 200 µL PBS (3 times) to remove unadhered treatment (control or exosomes). Coverslips were then read at a fluorescence excitation of 480 nm and emission of 500-700 nm with 2 nm steps. Finally, coverslips were placed on slides for fluorescence and brightfield imaging (Leica Fluorescence Microscope, 10X). At least three images were obtained for each coverslip. The fluorescence intensity was quantified using Fiji software. Briefly, the image was separated into color channels, the area selected, and the corrected total cell fluorescence (CTCF) was determined using the internal density and the area and mean fluorescence. A one-way ANOVA was performed to determine statistical significance.

Cell Culture:
MDA-MB-468 (triple-negative breast cancer lung metastasis, pleural effusion), MDA-MB-231 (triple-negative breast cancer lung metastasis pleural effusion), HCC 1806 (triple-negative, primary breast tumor) and HCC 1937 (triple-negative primary breast tumor) (TNBC) cell lines were purchased from American Type Culture Collection (ATCC). Cells were cultured in RPMI-1630 supplemented with 10% fetal bovine serum (Avantar Seradign). For normoxia, a humidified incubator containing 5% carbon dioxide, 21% oxygen, and 74% nitrogen at 37 °C was used. For hypoxia, a biospheric C21 hypoxic chamber supplemented with 2% oxygen, 93% nitrogen, and 5% carbon dioxide was used. Media was changed every 48 hours, and passage numbers were kept below 10 after receiving the cells from ATCC.

Flow Cytometry of MDA-MBA-468, MDA-MB-231, HCC 1937, and HCC 1806 cell lines for NRP1:
The cultured cells were removed from the plate and suspended in 500 µL of PBS and recombinant anti-NRP1 primary antibody (ab81321, Abcam.) Primary antibody was allowed to interact at room temperature for 30 minutes. Cells were then washed with PBS three times to remove the primary antibody via centrifuging at 1,200 g for 5 minutes. Goat anti-rabbit IgG H&L (FITC) antibody (ab6717, Abcam) was then added and allowed to rock at room temperature for 30 minutes. After 30 minutes, the secondary antibody was removed, and the cells were washed three times with PBS. Cells were resuspended in 500 µL of PBS, and flow cytometry was performed using a BD Accuri C6 Flow Cytometer. Twenty thousand events were captured for each sample with three replicates for each cell line.

Cellular Internalization:
Ten thousand cells were seeded into Biotek 8-well glass plates. Once adhered, media was changed to serum-free RPMI-1640. Cell nucleus stain (Invitrogen ReadyProbes NucBlue Live Reagent) was applied for nuclear monitoring. Doxorubicin (20 µM) encapsulated in exosomes (iDHRX or DExo) was added to well plates and imaged every 30 minutes for 24 h using the Lionheart FX (Biotek, USA) with DAPI with Texas Red filters. Texas Red fluorescence intensity was quantified using Fiji. The image was separated into color channels, the area selected, and the CTCF was determined using the internal density, area, and mean fluorescence.

Cytotoxicity:
Monolayer Cultures: Ten thousand MDA-MB-231, MDA-MB-468, HCC 1806, or HCC 1937 cells were seeded into 8 wells of 96-well clear-bottom plates. The cells were incubated 24 hours to allow attachment before placing them in either a normal oxygen incubator (20% oxygen) or a hypoxia chamber (2% oxygen) for 24 hours. Cells were then treated with either iDHRX, exosomes, or free doxorubicin for 48 hours, the media was removed, and cells were washed three times to remove any remaining treatment. Subsequently, 20 µL of Alamar Blue (10X, Invitrogen) and 180 µL of fresh medium were added. The absorbance was then measured at 570 nm, and viability was calculated using equation 1.

Equation 1:

$$\frac{(O2 \times A1) - (O1 \times A2)}{(O2 \times P1) - (O1 \times P2)} x\ 100$$

O1 = molar extinction coefficient (ε) of oxidized Alamar Blue at 570 nm (80,586)
O2 = ε of oxidized Alamar Blue at 600 nm (117,216)
A1 = absorbance of test wells at 570 nm
A2 = absorbance of test wells at 600 nm
P1 = absorbance of positive growth control well
P2 = absorbance of positive growth control well

Spheroid Cultures: Silicone molds were used to prepare spheroid scaffolds (Microtissues) using 2% agarose to create the "wells," following the manufacturer's protocol. Wells were seeded with 273,000 cells/190 µL to produce a spheroid with a diameter of at least 200-300 µm. The seeded scaffolds were incubated for 7 days, changing the RPMI-1640 with 10% FBS every 2 days. The scaffolds were then placed in either normoxic (20% oxygen) or hypoxic (2% oxygen) conditions for 24 h before respective treatments for 48 hours. Groups included no treatment, purified, unmodified exosomes encapsulating doxorubicin, free doxorubicin

(1.25 μM), or iDHRX (5 μM, 7 μM, and 10 μM). After treatment, the scaffolds were washed with PBS before viability was analyzed by Celltiter-Glo 3D cell viability assay (Promega). Luminescence (SpectraMax, M5, Molecular Devices) was measured, and viability was calculated according to the manufacturer's recommendations.

Depth of penetration in spheroid cultures:
The spheroids were allowed to grow for 7 days before treatment. Treatment groups control (no treatment), carboxyfluorescein, iHRX, free doxorubicin, or carboxyfluorescein-iDHRX. After 7 days of growth, half of the spheroids were put in a hypoxic environment. After 24 hours, 1.25 μM free doxorubicin or 10 μM iDHRX was added. Visual comparisons were made for treatments with 1.25 μM free doxorubicin and 10 μM iDHRX at 30 minutes, 1 hour, 2 hours, 6 hours, and 24 hours. Spheroids were then imaged using fluorescence microscopy (20X, Leica Fluorescence Scope). A z-stack of each spheroid was constructed (from top to bottom) using steps of 5 μm. Each spheroid was visualized using both a Texas red filter to show the accumulation of doxorubicin and a FITC filter to show the exosome accumulation.

3. Results and Discussion:

Characterization of modified exosomes:
Exosomes were isolated from raw bovine milk. The diameter of the isolated exosomes was determined using dynamic light scattering (DLS), atomic force microscopy (AFM), and high-resolution transmission electron microscopy (HRTEM) (Table 1). As a rapid validation of the reproducibility of the isolation and modification processes, DLS was used to confirm that the size of each exosome batch was within the literature reports (30-150 nm[48]). Literature suggests that long term storage at -80°C maintains stability of bovine milk exosomes.[49] However, we did not test the stability of the isolated exosomes beyond one week. To verify that the isolated extracellular vesicles are exosomes, flow cytometry for CD63 (a well-documented exosomal marker[30,35]) was performed (Figure S7). These results compare CD63 stained vs unstained exosomes, indicating that the nanovesicles are exosomes as opposed to other biological vesicles. The larger diameter for the HRX is likely due to incorporating the hypoxia-responsive lipid and the iRGD-peptide conjugate with the PEG groups.

An accurate evaluation of their concentration was essential before modifying the isolated exosomes or using them for in vitro experiments with cells. Hence, exosome preparations were quantified using a tunable resistive pulse sensing instrument, giving an average of 1.1×10^{13} exosomes/mL. Purified exosomes were first modified to release encapsulated contents under reducing conditions. A synthesized hypoxia-responsive lipid (Figure 2) was incorporated into the exosome bilayer. The incorporation of the orange-red lipid into the bilayer was confirmed by UV-Vis spectroscopy. After optimization, a 100 μM solution of lipid (80 μL) and exosomes (120 μL approximately 1.3×10^{12} exosomes) provided the highest lipid incorporation (9.2 μM, 32% efficiency). In addition to the hypoxia-responsive lipid, an iRGD peptide (DSPE-PEG_{5000}-iRGD; Figure 3) was incorporated. The spherical structure and size of the exosomes were then confirmed by AFM (Figure 4A), TEM (Table 1), and DLS (Table 1). Finally, doxorubicin, a chemotherapeutic, was encapsulated, giving a modified exosome (iDHRX). After incorporating the hypoxia-responsive lipid, DSPE-PEG_{5000}-iRGD modifications, and doxorubicin encapsulation, the exosomes were at a concentration of 5×10^{12} particles/mL (Figure 5B). The presence of DSPE-PEG_{5000}-iRGD on the HRX was confirmed through adhesion assay and exosome structure through AFM. AFM can be used as a complementary tool to image a variety of biomolecules at high lateral resolution, revealing structural details and conformational changes in real time and in physiological conditions. Doxorubicin encapsulation and efficiency [(65 $\pm$ 6)%, 90 μM] after washing and determination through UV-Vis spectroscopy.

Table 1. Sizes of exosomes and hypoxia-responsive exosomes (HRX) by dynamic light scattering (DLS), atomic force microscopy (AFM), and high-resolution transmission microscopy (HRTEM).

	DLS Size (nm)	PDI	AFM (nm)	HRTEM (nm)
Isolated exosomes	52 ± 15	0.26 ± 0.08	60 ±10	40 ± 20
HRX	119 ± 24	0.23 ± 0.02	130 ±10	130 ± 20

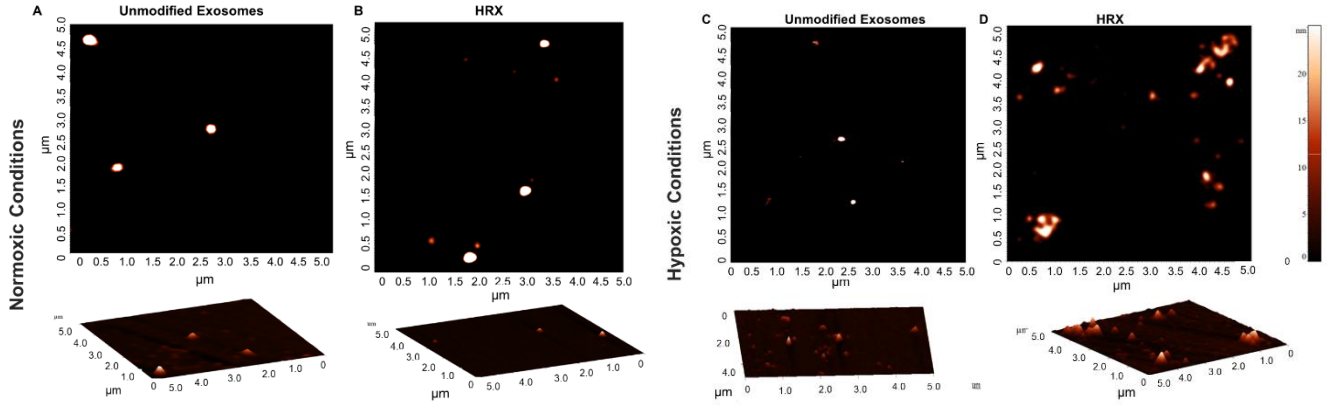

Figure 4. Atomic force microscopy images of unmodified exosomes and HRXs under normoxia and hypoxia (2% Oxygen). Fragments of the HRXs with an approximate size of 25 nm were observed in hypoxic (2% Oxygen) conditions (**A**) Unmodified exosomes in normoxic conditions, showing whole spheres. (**B**) HRX in normoxic conditions, showing whole spheres. (**C**) Unmodified exosomes in hypoxic (2% Oxygen)conditions, showing whole spheres. (**D**) HRXs in hypoxic (2% Oxygen) conditions, showing fragmented pieces.

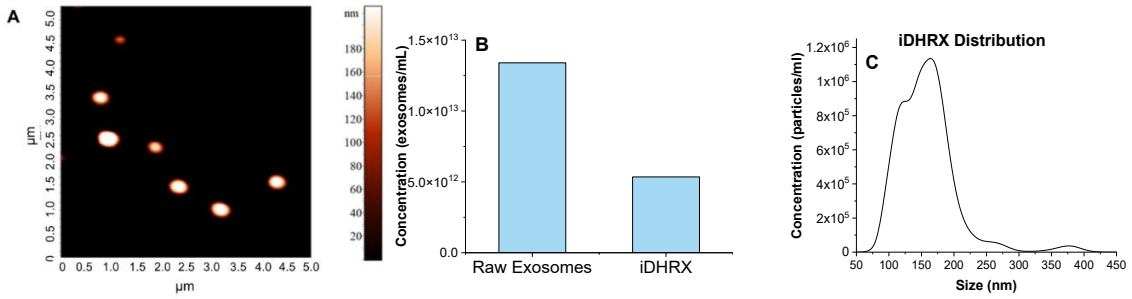

Figure 5. (**A**) AFM of iDHRX. The size range of exosomes 50 nm - 200 nm. (**B**) Particle counting for raw bovine milk exosomes and iDHRX. (**C**) The size distribution of iDHRX using Tunable Resistive Pulse Sensing. The mode is 149 ± 7 nm, and the mean is 167 ± 2 nm.

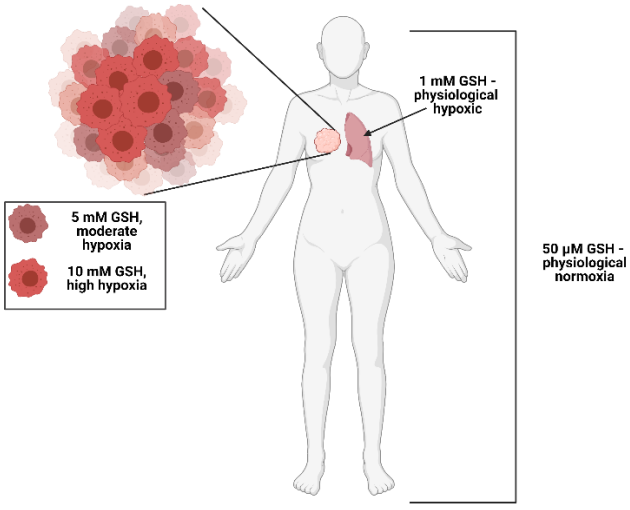

Figure 6: Glutathione (GSH) levels throughout the body; 50 µM GSH is physiological normoxia, 1 mM GSH is physiological hypoxia, 5 mM GSH is moderate hypoxia, and 10 mM GSH is high hypoxia.

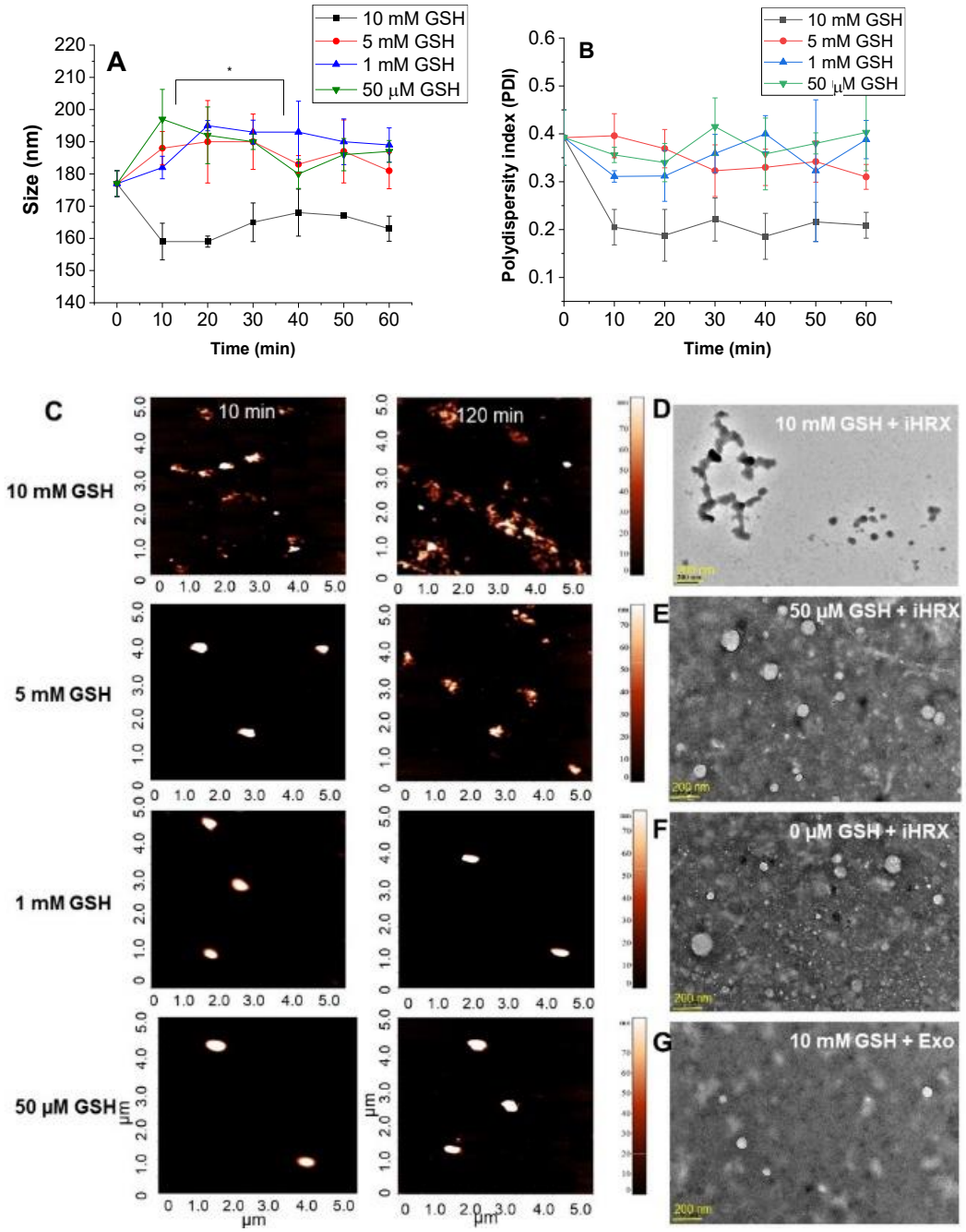

Figure 7. Size and shape of iHRX in the presence of glutathione. (**A**) Hydrodynamic diameters of HRX from 0 – 120 min in 10 min increments with increasing amounts of glutathione. (**B**) polydispersity indices of HRX from 0 – 120 min in 10 min increments with increasing amounts of glutathione. (**C**) AFM images of HRX at 10 min (left) and 120 min (right). (**D**) HR-TEM images of iHRX with 10 mM glutathione at 120 min. (**E**) HR-TEM images of iHRX with 50 µM glutathione at 120 min. **(F)** HR-TEM images of iHRX with 0M glutathione at 120 min. **(G)** HR-TEM images of exosomes with 10 mM glutathione at 120 min.

The reduction of the modified exosomes (iHRX) was determined using glutathione concentrations from 50 µM to 10 mM (Figure 6).[46,47,50] With 10 mM glutathione, modified exosomes broke into fragments within 10 minutes of exposure. After 2 hours, exosomes exposed to 5 mM glutathione were fragmented. At concentrations less than 5 mM glutathione, HRX fragmentation was not observed (Figure 7). Notably,10 mM glutathione is typically found within most hypoxic niches of the tumors. The 5 mM glutathione is observed within the tumor's exterior margins during the transition to hypoxia and is significantly higher than other tissue within the body (1 mM to 50 µM).[46,47,50] This fragmentation of exosomes at 10 mM glutathione with minimal fragmentation at 5 mM glutathione indicates that exosomes modified with a hypoxia-responsive lipid will only break under a reducing environment mimicking the hypoxic niches of solid tumors.

While incorporating the hypoxia-responsive lipid provides a trigger to release the exosome-encapsulated payload, incorporation of iRGD peptide is essential for targeting, tumor

penetration, and cellular internalization. A surface-adhesion assay was developed to confirm DSPE-PEG_{5000}-iRGD in the modified exosomes. The iRGD peptide interacts with $\alpha_v\beta_3$ integrin and NRP-1, both upregulated on cancer cells and facilitates targeting and penetration of the exosomes (illustrated in Figure 8).[51–55] To visualize the iRGD peptide integrated into the exosomes' lipid bilayer, DSPE-PEG_{5000}-FITC was incorporated into iHRX (CF-iHRX) and exosomes. The surface of the slides were coated with the $\alpha_v\beta_3$ integrin allowing for iRGD peptide to attach to the surface. There was a significant increase (1.5-2 fold) in fluorescence intensity in CF-iHRX compared to the unmodified exosomes (Figure 9). These results verified that the iRGD peptide was incorporated in the exosome bilayer.

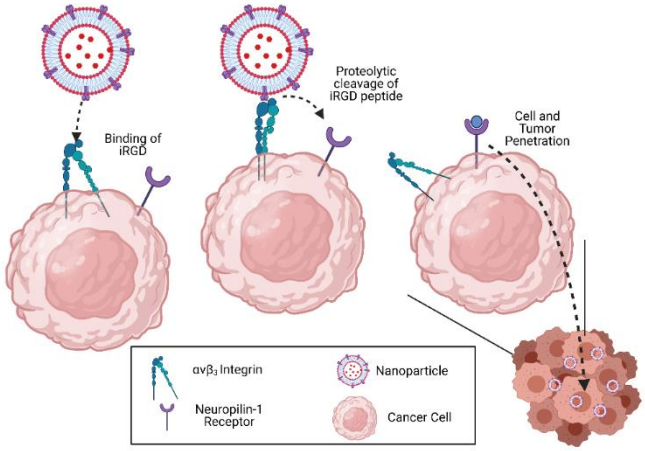

Figure 8. Mechanisms of iRGD peptide. The iRGD peptide binds to $\alpha_v\beta_3$ integrin receptor. Subsequent proteolytic cleavage allows binding to the NRP-1 receptor and penetration into the solid tumors.[41,44]

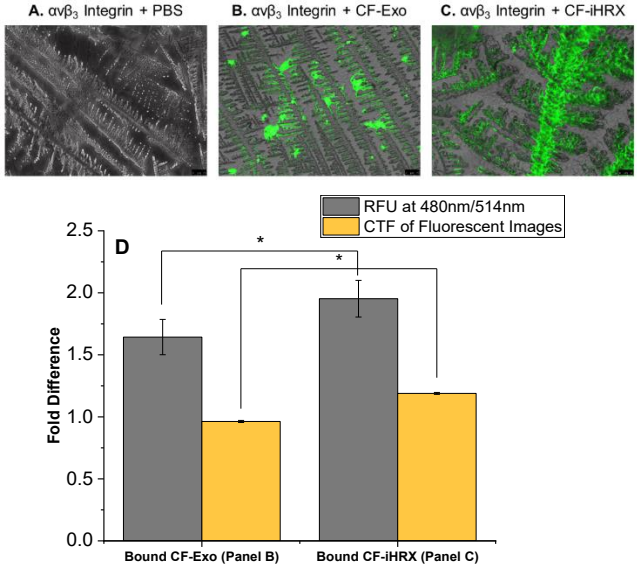

Figure 9. Adhesion assay of $\alpha_v\beta_3$ to iRGD peptide. Fluorescence images for (**A**) $\alpha_v\beta_3$ Integrin and PBS, (**B**) $\alpha_v\beta_3$ integrin and exosomes, and (**C**) $\alpha_v\beta_3$ integrin and iHRX. (**D**) Corrected total fluorescence and fluorescence signal show significant differences for both methods. N =12 and P-values <0.001.

Cellular studies:

NRP1 expression in TNBC cells: Due to the crucial requirement of NRP1 expression for the penetration of nanoparticles, its expression in the cell lines was confirmed by flow cytometry (Figure 10). Flow cytometry indicated that MDA-MB-231 cells had increased NRP1 expression in hypoxic (2% Oxygen) conditions, while HCC 1937 cells showed increased NRP1 expression in normoxic conditions. The NRP1 expression difference between normoxia and hypoxia on the cells implies that certain cell lines may be more susceptible to iHRX drug delivery.

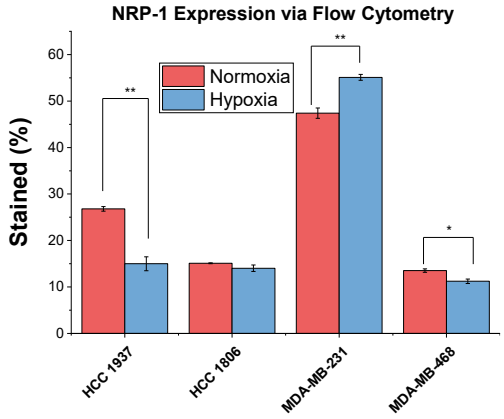

Figure 10. NRP1 expression as determined by flow cytometry for HCC 1937, HCC 1806, MDA-MB-231, and MDA-MB-468 cells in normoxia and hypoxia (2% Oxygen).

Cellular internalization and cytotoxicity for monolayer cultures normoxia: Internalization of iRGD-exosomes (iDHRX) into MDA-MB-468, MDA-MB-231, HCC 1806, and HCC 1937 TNBC cells was monitored for 24 hours (Figure 11). iDHRX showed higher internalization after 2 hours compared to doxorubicin-encapsulated exosomes without the iRGD peptide (DExo) (Figure 11). Within the two hours after treating TNBC cells with doxorubicin in any form (free, encapsulated in unmodified exosomes, or encapsulated in modified exosomes), the intensity of DAPI began to decrease indicating cell death. Treating both HCC 1937 and MDA-MB-468 cells with iDHRX showed a quantifiable and significant difference in DAPI intensity, likely attributed to the multiple uptake pathways of exosomes. For example, HCC 1937 cells have higher exosomal uptake compared to other cell lines regardless of NRP-1 and $\alpha_v\beta_3$ integrin expression levels in a 2D monolayer environment.[56–58] Labeling of the exosomes and higher magnification of individual cells would have increased resolution and may have allowed a more direct measurement of doxorubicin uptake, allowing a more mechanistic evaluation of cell line specific uptake. Regardless of the mechanism, exosomes, modified and unmodified, are being taken up by the cells and appear to be killing the cells within 2 hours, similar to free doxorubicin (Figure 11). Additional studies, such as evaluating DNA damage, looking for apoptotic bodies, or determining the level and function of topoisomerase II, to measure cell death at these early time points would assist in determining the mechanisms of cells death in the initial stages of internalization.[56]

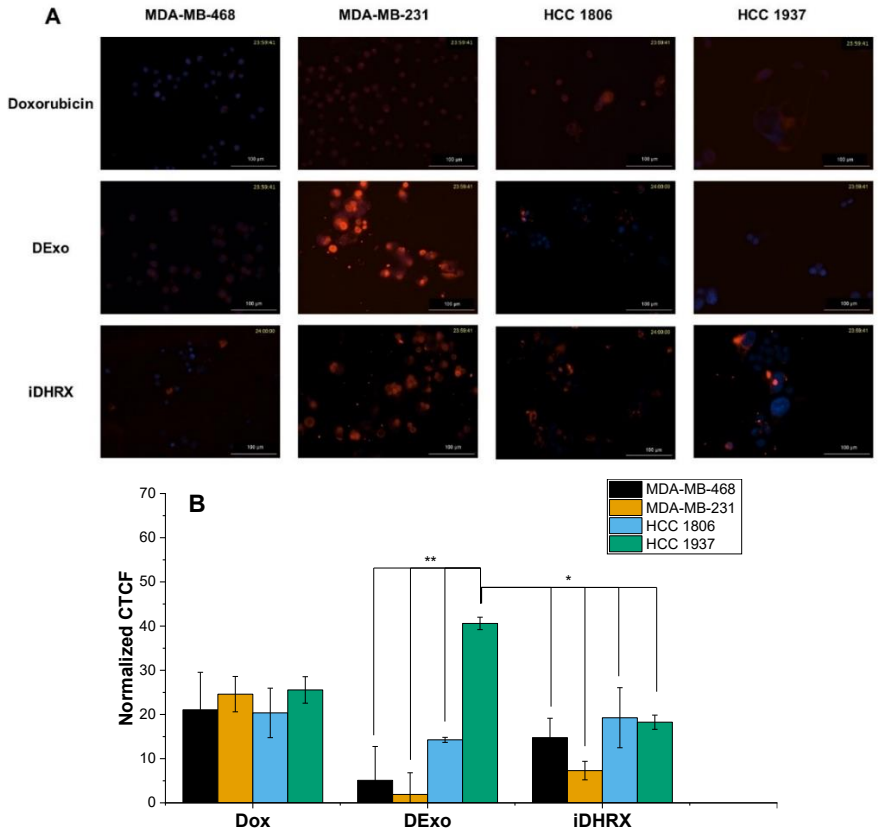

Figure 11. (**A**) Cellular Internalization for MDA-MB-468, MDA-MB-231, HCC 1806, and HCC 1937. (**B**) Quantification of internalization based on the intensity of doxorubicin. Only HCC 1937 cells show significant uptake when comparing doxorubicin, doxorubicin encapsulated exosomes (DExo) and iDHRX. N = 3, * $p<0.05$, ** $p<0.001$.

Monolayer cytotoxicity results for the four cell lines indicated significant ($p < 0.001$) cell death when treated with iDHRX compared to both unmodified exosomes and no treatment controls (Figure 12). Doxorubicin concentrations of 0.5 μM to 20 μM in iDHRX were tested with MDA-MB-468, HCC 1806, and HCC 1937 cells. The lowest concentration of iDHRX to show significance amongst each cell line is reported. EC_{50} values (Table 2) were calculated for each cell line based on these cytotoxicity results. As expected, HCC 1937 cells had increased EC_{50} values compared to other cell lines tested. [57] The variability of the EC_{50} and effectiveness of treatment is likely due to genetic variability and protein expression on the cells. Additionally, the lack of tumor microenvironment and cellular interactions can also affect the effectiveness of treatment, indicating a need for 3D spheroid viability and penetration studies.

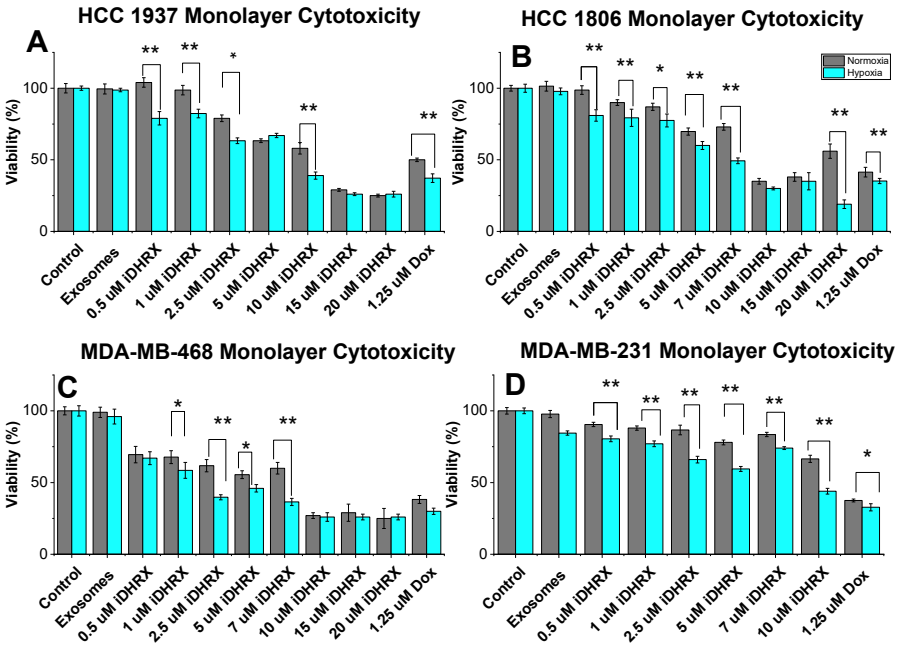

Figure 12. Monolayer cytotoxicity for (**A**) HCC 1937, (**B**) HCC 1806, (**C**) MDA-MB-468, and (**D**) MDA-MB-231 cells (n = 24). * $p < 0.05$, ** $p < 0.001$. Normoxia is shown in grey and hypoxia (2% Oxygen) depicted in blue.

Table 2: Monolayer EC_{50} values in normoxia and hypoxia.

Cell line	EC_{50} normoxia (μM)	EC_{50} hypoxia (μM)
MDA-MB-231	5.2 ± 0.4	3.7± 0.7
MDA-MB-468	6.1 ± 2.2	4.9 ± 0.3
HCC 1806	6.7 ± 1.4	6.9 ± 1.8
HCC 1937	9.0 ± 1.7	6.3 ± 1.8

Spheroid cytotoxicity and penetration depth: A 3D spheroid cytotoxicity assay indicated less cell death than monolayer cultures (Figure 13). For spheroids, a hypoxic gradient begins to form at 200 μm, allowing external hypoxia conditions to serve as a control.[23,58,59] Consequently, the spheroids showed similar viability in both hypoxia and normoxia. MDA-MB cells showed more significant death at several doses compared to HCC cells. HCC 1937 spheroids showed significant cell death at 10 μM iDHRX and 1.25 μM doxorubicin and showed the least effective treatment compared to other cell lines. This is likely due to the efflux pumps and doxorubicin resistance often found in the HCC 1937 cells.[57,60,61] EC_{50} values (Table 3) were calculated for spheroid cultures and indicated equivalent tox slightly higher values to that of monolayer EC_{50} values.

.

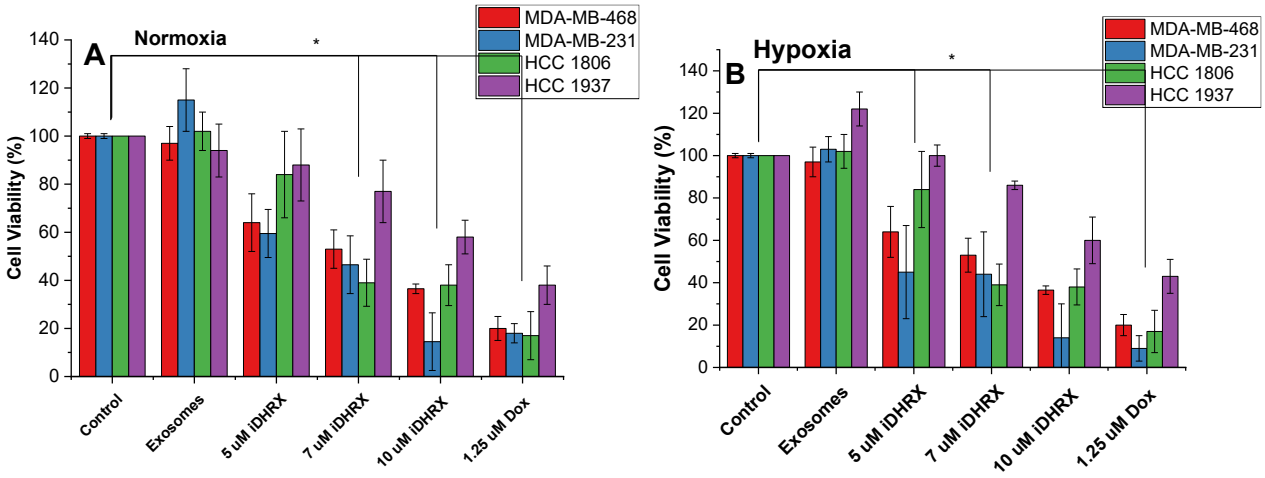

Figure 13. Spheroid viability for HCC 1806 (green), HCC 1937 (purple), MDA-MB-468 (red), and MDA-MB-231 (blue) triple-negative breast cancer cell lines. Each cell line was treated in a normoxic (**A**) and hypoxic (2% Oxygen) (**B**) environment for 48 hours. N = 3 *p<0.05

Table 3: Spheroid EC_{50} values normoxia and hypoxia.

Cell line	EC_{50} normoxia (μM)	EC_{50} hypoxia (μM)
MDA-MB-231	7.1 ± 3.1	8.2 ± 1.2
MDA-MB-468	4.4 ± 0.8	5.9 ± 1.8
HCC 1806	6.7 ± 2.6	6.9 ± 0.7
HCC 1937	10.4 ± 2.6	9.9 ±0.9

Analyses of the depth of penetration of iDHRX in the cultured spheroids were performed by confocal fluorescence microscopy. iDHRX reached the center of the 3D spheroids within 1 hour, while free doxorubicin does not reach the same levels until at least 2 hours. By 6 hours, the penetration levels become steady, indicating an equilibrium between the interior and exterior of the 3D spheroid has been reached for both free doxorubicin and iDHRX. (Figure 14 and 15)

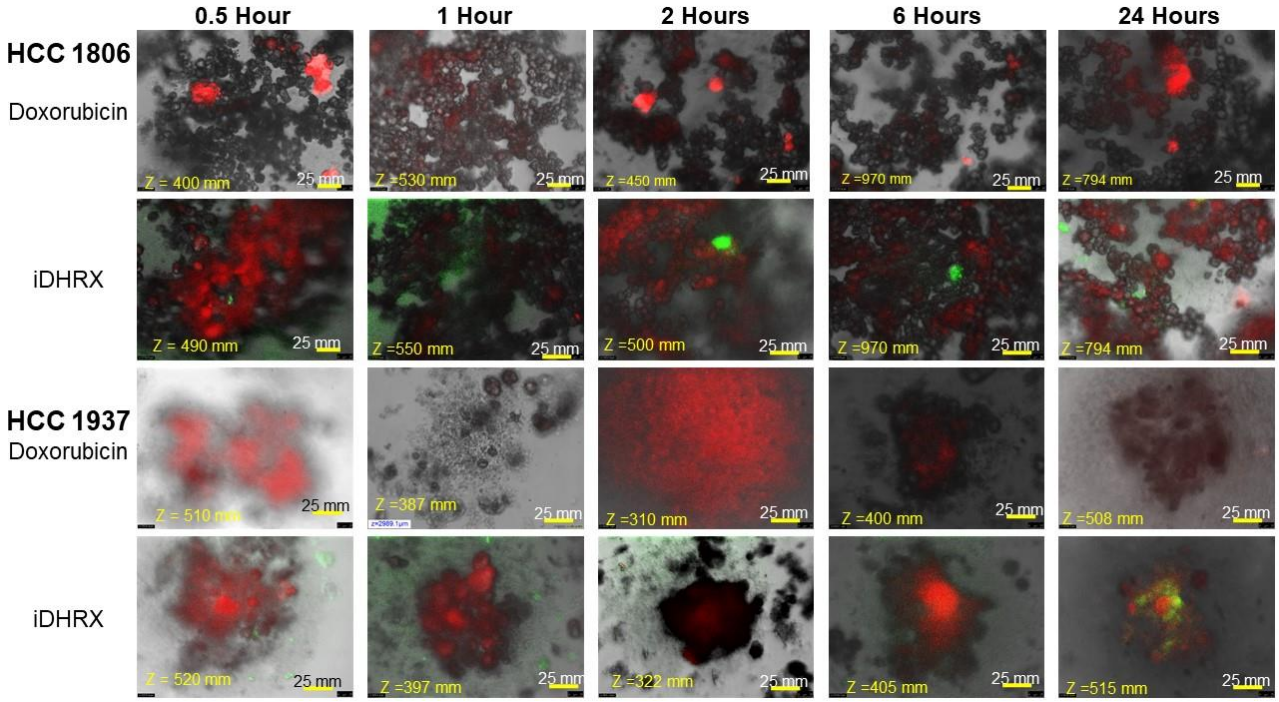

Figure 14. Penetration of doxorubicin and iDHRX in the spheroids of HCC 1806 and HCC 1937 cell spheroids. Doxorubicin was visualized using Texas red fluorescence filter. Exosomes were visualized using a FITC filter. Each image is taken at the focus depth, each slice is 5 μm thick.

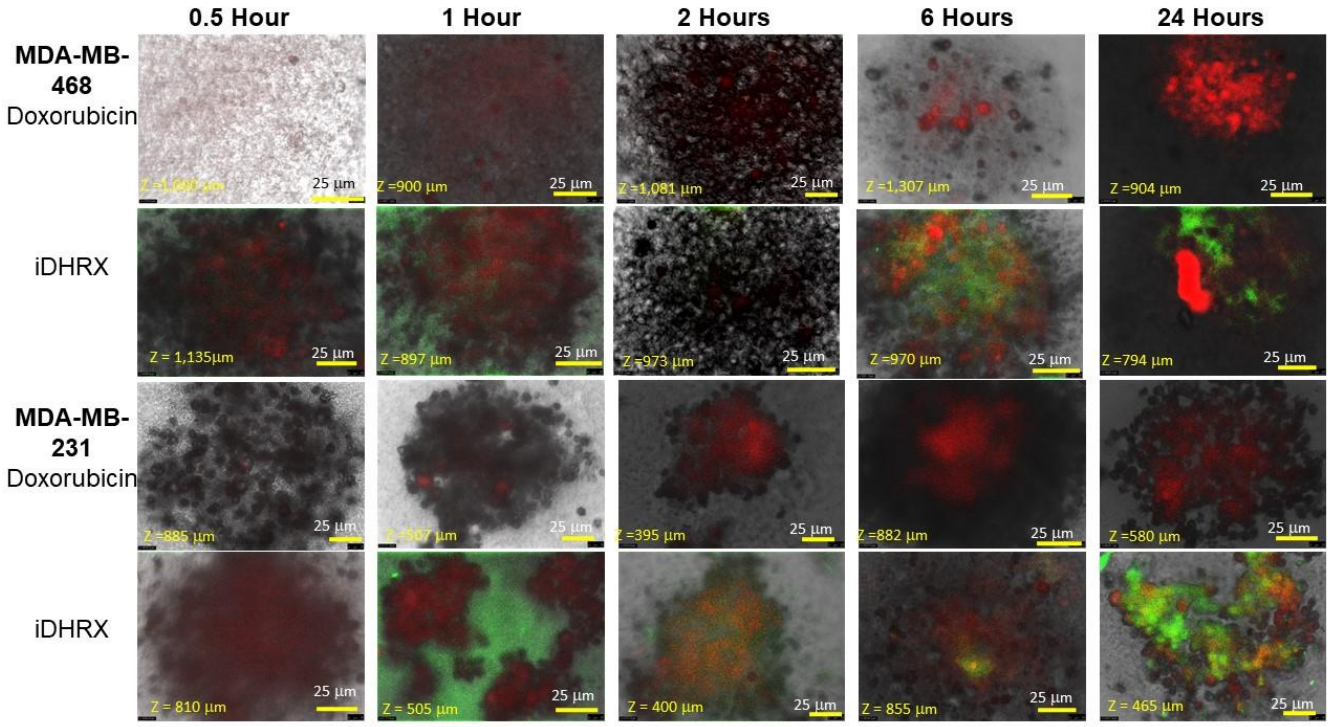

Figure 15. Penetration of doxorubicin and iDHRX in the MDA-MB-468 and MDA-MB-231 cell spheroids. Doxorubicin was visualized using Texas red fluorescence filter. Exosomes were visualized using a FITC filter. Each image is taken at the focus depth, each slice is 5 µm thick.

Comparative analysis of primary versus metastatic cells: A statistical analysis of all spheroids' iDHRX treatments was performed. At 10 µM iDHRX treatment, cell viability was highest for HCC 1937 spheroids (58%, Figure 14) and lowest for MDA-MB-231 spheroids (14%, Figure 15). Overall, HCC 1937 cell spheroids showed increased viability than the others, possibly due to the doxorubicin resistance for this primary tumor-derived cell line.[62] The MDA-MB-231 and MDA-MB-468 cells showed decreased cell viability, indicating they respond better to doxorubicin and the iDHRX treatment in an *in vitro* tumor microenvironment (Figure 16).

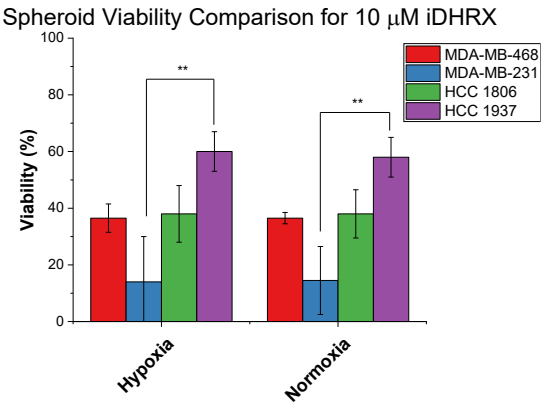

Figure 16. Spheroid cytotoxicity comparison between metastatic and primary tumor sites for iDHRX in normoxia and hypoxia. N = 3 * p <0.05, ** p<0.001

4. Conclusion:

Bovine milk exosomes have been successfully modified for active targeting to NRP-1 and hypoxia sensitivity, and a chemotherapeutic agent was then encapsulated. The hypoxia-responsive lipid and iRGD peptide modifications facilitated the delivery of doxorubicin to triple-negative breast cancer cells. The modified exosomes fragment in hypoxia (2% or less oxygen), causing the encapsulated doxorubicin to release. The iRGD peptide on the surface allowed the exosomes to penetrate the spheroids of the breast cancer cells. The released doxorubicin showed significant cytotoxicity in monolayer and spheroid cultures of the four different triple-negative breast cancer cell lines.

ASSOCIATED CONTENT

Supporting Information. Schematic of exosome isolation, C-18 reverse-phase HPLC and ESI Mass spectroscopy of iRGD peptide, CD spectrum for DSPE-PEG_{5000}-iRGD, 1H NMR and ESI Mass spectroscopy of hypoxia-responsive lipid, flow cytometry analysis of NRP-1 expression of the four TNBC cell lines, flow cytometry analysis of CD63 expression on exosomes.

AUTHOR INFORMATION

Corresponding Author

* Sanku Mallik - Department of Pharmaceutical Sciences, North Dakota State University, Fargo, North Dakota; Phone: 701-231- 7888; Email: Sanku.mallik@ndsu.edu; Fax: 701-231-7831.

Author Contributions

JP contributed to experimental design, performed experiments, and wrote the manuscript. SM, SV, KS YC, and AB contributed to experimental design and writing the manuscript. KD, SB, LF, LA, JF, JO, TM, assisted in performing experiments and experimental design.

The manuscript was written through contributions of all authors. All authors have given approval to the final version of the manuscript.

Funding Sources

S.M., VS, and K.S. acknowledge support from NIH (NIGMS) grant 2R01GM 114080. S.M. also acknowledges partial supports from NIH grant U54 GM12872.

Notes

The authors declare no competing financial interest.

ACKNOWLEDGMENT

S.M., VS, and K.S. acknowledge support from NIH (NIGMS) grant 2R01GM 114080. S.M. also acknowledges partial supports from NIH grant U54 GM12872. Any opinions, findings, and conclusions or recommendations expressed in this material are those of the author(s) and do not necessarily reflect the views of the NSF. Authors would also like to acknowledge Biorender.com for assistance with graphics.

ABBREVIATIONS

3D, Three-dimensional; AFM, Atomic Force Microscopy; ANOVA, Analysis of Variance; CTCF, corrected total cell fluorescence; DExo, doxorubicin encapsulated exosomes; DLS, Dynamic light scattering; Exo, exosomes; FBS, fetal bovine serum; FITC, fluorescein isothiocyanate; GSH, glutathione; HOBt, hydroxybenzotriazole; HR-TEM, high-resolution transmission electron microscopy; HRX, hypoxia responsive exosomes; iDRHX, iRGD-doxorubicin encapsulated-hypoxia responsive exosomes; iHRX, iRGD-hypoxia responsive exosomes; iRGD, cyclized arginine-glycine-aspartic acid peptide; NRP-1, neuropilin-1 receptor; PBS, phosphate buffer saline; PDI, polydispersity index; rpm, revolutions per minute; xg, g forces.

REFERENCES

(1) Siegel, R. L.; Miller, K. D.; Jemal, A. Cancer Statistics, 2020. CA: A Cancer Journal for Clinicians 2020, 70 (1), 7–30. https://doi.org/10.3322/caac.21590.

(2) Triple-negative Breast Cancer | Details, Diagnosis, and Signs https://www.cancer.org/cancer/breast-cancer/understanding-a-breast-cancer-diagnosis/types-of-breast-cancer/triple-negative.html (accessed 2021 -03 -18).

(3) Goldman, E.; Zinger, A.; da Silva, D.; Yaari, Z.; Kajal, A.; Vardi-Oknin, D.; Goldfeder, M.; Schroeder, J. E.; Shainsky-Roitman, J.; Hershkovitz, D.; Schroeder, A. Nanoparticles Target Early-Stage Breast Cancer Metastasis in Vivo. Nanotechnology 2017, 28 (43), 43LT01. https://doi.org/10.1088/1361-6528/aa8a3d.

(4) Jamdade, V. S.; Sethi, N.; Mundhe, N. A.; Kumar, P.; Lahkar, M.; Sinha, N. Therapeutic Targets of Triple-Negative Breast Cancer: A Review. Br J Pharmacol 2015, 172 (17), 4228–4237. https://doi.org/10.1111/bph.13211.

(5) da Silva, J. L.; Cardoso Nunes, N. C.; Izetti, P.; de Mesquita, G. G.; de Melo, A. C. Triple Negative Breast Cancer: A Thorough Review of Biomarkers. Critical Reviews in Oncology/Hematology 2020, 145, 102855. https://doi.org/10.1016/j.critrevonc.2019.102855.

(6) Tzikas, A.-K.; Nemes, S.; Linderholm, B. K. A Comparison between Young and Old Patients with Triple-Negative Breast Cancer: Biology, Survival and Metastatic Patterns. Breast Cancer Res Treat 2020, 182 (3), 643–654. https://doi.org/10.1007/s10549-020-05727-x.

(7) Sharma, P. Biology and Management of Patients With Triple-Negative Breast Cancer. Oncologist 2016, 21 (9), 1050–1062. https://doi.org/10.1634/theoncologist.2016-0067.

(8) Lyons, T. G. Targeted Therapies for Triple-Negative Breast Cancer. Curr. Treat. Options in Oncol. 2019, 20 (11), 82. https://doi.org/10.1007/s11864-019-0682-x.

(9) Joiner, M. C.; Kogel, A. J. van der. Basic Clinical Radiobiology; CRC Press, 2018.

(10) Soltani, M.; Chen, P. Effect of Tumor Shape and Size on Drug Delivery to Solid Tumors. Journal of Biological Engineering 2012, 6 (1), 4. https://doi.org/10.1186/1754-1611-6-4.

(11) Soltani, M.; Chen, P. Numerical Modeling of Fluid Flow in Solid Tumors. PLoS One 2011, 6 (6), e20344. https://doi.org/10.1371/journal.pone.0020344.

(12) Kim, Y.; Stolarska, M. A.; Othmer, H. G. The Role of the Microenvironment in Tumor Growth and Invasion. Prog Biophys Mol Biol 2011, 106 (2), 353–379. https://doi.org/10.1016/j.pbiomolbio.2011.06.006.

(13) Belli, C.; Trapani, D.; Viale, G.; D'Amico, P.; Duso, B. A.; Della Vigna, P.; Orsi, F.; Curigliano, G. Targeting the Microenvironment in Solid Tumors. Cancer Treatment Reviews 2018, 65, 22–32. https://doi.org/10.1016/j.ctrv.2018.02.004.

(14) Bender, R. J.; Gabhann, F. M. Expression of VEGF and Semaphorin Genes Define Subgroups of Triple Negative Breast Cancer. PLOS ONE 2013, 8 (5), e61788. https://doi.org/10.1371/journal.pone.0061788.

(15) Naik, A.; Al-Zeheimi, N.; Bakheit, C. S.; Al Riyami, M.; Al Jarrah, A.; Al Moundhri, M. S.; Al Habsi, Z.; Basheer, M.; Adham, S. A. Neuropilin-1 Associated Molecules in the Blood Distinguish Poor Prognosis Breast Cancer: A Cross-Sectional Study. Sci Rep 2017, 7. https://doi.org/10.1038/s41598-017-03280-0.

(16) Darvishi, B.; Boroumandieh, S.; Majidzadeh-A, K.; Salehi, M.; Jafari, F.; Farahmand, L. The Role of Activated Leukocyte Cell Adhesion Molecule (ALCAM) in Cancer Progression, Invasion, Metastasis and Recurrence: A Novel Cancer Stem Cell Marker and Tumor-Specific Prognostic Marker. Experimental and Molecular Pathology 2020, 104443. https://doi.org/10.1016/j.yexmp.2020.104443.

(17) Mani, S. A.; Guo, W.; Liao, M.-J.; Eaton, E. Ng.; Ayyanan, A.; Zhou, A. Y.; Brooks, M.; Reinhard, F.; Zhang, C. C.; Shipitsin, M.; Campbell, L. L.; Polyak, K.; Brisken, C.; Yang, J.; Weinberg, R. A. The Epithelial-Mesenchymal Transition Generates Cells with Properties of Stem Cells. Cell 2008, 133 (4), 704–715. https://doi.org/10.1016/j.cell.2008.03.027.

(18) Park, S.-Y.; Choi, J.-H.; Nam, J.-S. Targeting Cancer Stem Cells in Triple-Negative Breast Cancer. Cancers (Basel) 2019, 11 (7), 965. https://doi.org/10.3390/cancers11070965.
(19) Morel, A.-P.; Lièvre, M.; Thomas, C.; Hinkal, G.; Ansieau, S.; Puisieux, A. Generation of Breast Cancer Stem Cells through Epithelial-Mesenchymal Transition. PLoS One 2008, 3 (8), e2888. https://doi.org/10.1371/journal.pone.0002888.
(20) Rahman, S. M.; Campbell, J. M.; Coates, R. N.; Render, K. M.; Byrne, C. E.; Martin, E. C.; Melvin, A. T. Evaluation of Intercellular Communication between Breast Cancer Cells and Adipose-Derived Stem Cells via Passive Diffusion in a Two-Layer Microfluidic Device. Lab Chip 2020, 20 (11), 2009–2019. https://doi.org/10.1039/D0LC00142B.
(21) Kong, D.; Hughes, C. J.; Ford, H. L. Cellular Plasticity in Breast Cancer Progression and Therapy. Front. Mol. Biosci. 2020, 7. https://doi.org/10.3389/fmolb.2020.00072.
(22) Reynolds, D. S.; Tevis, K. M.; Blessing, W. A.; Colson, Y. L.; Zaman, M. H.; Grinstaff, M. W. Breast Cancer Spheroids Reveal a Differential Cancer Stem Cell Response to Chemotherapeutic Treatment. Scientific Reports 2017, 7 (1), 10382. https://doi.org/10.1038/s41598-017-10863-4.
(23) McKeown, S. R. Defining Normoxia, Physoxia and Hypoxia in Tumours—Implications for Treatment Response. Br J Radiol 2014, 87 (1035), 20130676. https://doi.org/10.1259/bjr.20130676.
(24) Kulkarni, P.; Haldar, M. K.; Katti, P.; Dawes, C.; You, S.; Choi, Y.; Mallik, S. Hypoxia Responsive, Tumor Penetrating Lipid Nanoparticles for Delivery of Chemotherapeutics to Pancreatic Cancer Cell Spheroids. Bioconjug Chem 2016, 27 (8), 1830–1838. https://doi.org/10.1021/acs.bioconjchem.6b00241.
(25) Sharma, A.; Arambula, J. F.; Koo, S.; Kumar, R.; Singh, H.; Sessler, J. L.; Kim, J. S. Hypoxia-Targeted Drug Delivery. Chem. Soc. Rev. 2019, 48 (3), 771–813. https://doi.org/10.1039/C8CS00304A.
(26) Sugahara, K. N.; Teesalu, T.; Karmali, P. P.; Kotamraju, V. R.; Agemy, L.; Girard, O. M.; Hanahan, D.; Mattrey, R. F.; Ruoslahti, E. Tissue-Penetrating Delivery of Compounds and Nanoparticles into Tumors. Cancer Cell 2009, 16 (6), 510–520. https://doi.org/10.1016/j.ccr.2009.10.013.
(27) Zhang, Y.-R.; Lin, R.; Li, H.-J.; He, W.; Du, J.-Z.; Wang, J. Strategies to Improve Tumor Penetration of Nanomedicines through Nanoparticle Design. Wiley Interdisciplinary Reviews: Nanomedicine and Nanobiotechnology 2018, 0 (0), e1519. https://doi.org/10.1002/wnan.1519.
(28) Kadonosono, T.; Yamano, A.; Goto, T.; Tsubaki, T.; Niibori, M.; Kuchimaru, T.; Kizaka-Kondoh, S. Cell Penetrating Peptides Improve Tumor Delivery of Cargos through Neuropilin-1-Dependent Extravasation. Journal of Controlled Release 2015, 201, 14–21. https://doi.org/10.1016/j.jconrel.2015.01.011.
(29) Pullan, J. E.; Shreffler, J. W.; Dailey, K. M.; Mallik, S.; Brooks, A. E. Overcoming Hurdles in Nanoparticle Clinical Translation: The Influence of Experimental Design and Surface Modification. International Journal of Molecular Sciences 2019, 20 (23), 6056. https://doi.org/10.3390/ijms20236056.
(30) Munagala, R.; Aqil, F.; Jeyabalan, J.; Gupta, R. C. Bovine Milk-Derived Exosomes for Drug Delivery. Cancer Lett 2016, 371 (1), 48–61. https://doi.org/10.1016/j.canlet.2015.10.020.
(31) De Toro, J.; Herschlik, L.; Waldner, C.; Mongini, C. Emerging Roles of Exosomes in Normal and Pathological Conditions: New Insights for Diagnosis and Therapeutic Applications. Front. Immunol. 2015, 6. https://doi.org/10.3389/fimmu.2015.00203.
(32) Corrado, C.; Raimondo, S.; Chiesi, A.; Ciccia, F.; De Leo, G.; Alessandro, R. Exosomes as Intercellular Signaling Organelles Involved in Health and Disease: Basic Science and Clinical Applications. Int J Mol Sci 2013, 14 (3), 5338–5366. https://doi.org/10.3390/ijms14035338.
(33) Azmi, A. S.; Bao, B.; Sarkar, F. H. Exosomes in Cancer Development, Metastasis and Drug Resistance: A Comprehensive Review. Cancer Metastasis Rev 2013, 32 (0), 623–642. https://doi.org/10.1007/s10555-013-9441-9.
(34) Becker, A.; Thakur, B. K.; Weiss, J. M.; Kim, H. S.; Peinado, H.; Lyden, D. Extracellular Vesicles in Cancer: Cell-to-Cell Mediators of Metastasis. Cancer Cell 2016, 30 (6), 836–848. https://doi.org/10.1016/j.ccell.2016.10.009.
(35) Samuel, M.; Chisanga, D.; Liem, M.; Keerthikumar, S.; Anand, S.; Ang, C.-S.; Adda, C. G.; Versteegen, E.; Jois, M.; Mathivanan, S. Bovine Milk-Derived Exosomes from Colostrum Are Enriched with Proteins Implicated in Immune Response and Growth. Scientific Reports 2017, 7 (1), 5933. https://doi.org/10.1038/s41598-017-06288-8.
(36) Qian, R.; Jing, B.; Jiang, D.; Gai, Y.; Zhu, Z.; Huang, X.; Gao, Y.; Lan, X.; An, R. Multi-Antitumor Therapy and Synchronous Imaging Monitoring Based on Exosome. Eur J Nucl Med Mol Imaging 2022, Epub ahead of print. https://doi.org/10.1007/s00259-022-05696-x.
(37) Kang, T.; Gao, X.; Hu, Q.; Jiang, D.; Feng, X.; Zhang, X.; Song, Q.; Yao, L.; Huang, M.; Jiang, X.; Pang, Z.; Chen, H.; Chen, J. INGR-Modified PEG-PLGA Nanoparticles That Recognize Tumor Vasculature and Penetrate Gliomas. Biomaterials 2014, 35 (14), 4319–4332. https://doi.org/10.1016/j.biomaterials.2014.01.082.
(38) Alberici, L.; Roth, L.; Sugahara, K. N.; Agemy, L.; Kotamraju, V. R.; Teesalu, T.; Bordignon, C.; Traversari, C.; Rizzardi, G.-P.; Ruoslahti, E. De Novo Design of a Tumor-Penetrating Peptide. Cancer Res 2013, 73 (2), 804–812. https://doi.org/10.1158/0008-5472.CAN-12-1668.
(39) Sun, Q.; Ojha, T.; Kiessling, F.; Lammers, T.; Shi, Y. Enhancing Tumor Penetration of Nanomedicines. Biomacromolecules 2017, 18 (5), 1449–1459. https://doi.org/10.1021/acs.biomac.7b00068.
(40) Diaz Bessone, M. I.; Simón-Gracia, L.; Scodeller, P.; Ramirez, M. de los A.; Lago Huvelle, M. A.; Soler-Illia, G. J. A. A.; Simian, M. IRGD-Guided Tamoxifen Polymersomes Inhibit Estrogen Receptor Transcriptional Activity and Decrease the Number of Breast Cancer Cells with Self-Renewing Capacity. J Nanobiotechnology 2019, 17. https://doi.org/10.1186/s12951-019-0553-4.
(41) Liu, X.; Jiang, J.; Ji, Y.; Lu, J.; Chan, R.; Meng, H. Targeted Drug Delivery Using IRGD Peptide for Solid Cancer Treatment. Mol. Syst. Des. Eng. 2017, 2 (4), 370–379. https://doi.org/10.1039/C7ME00050B.
(42) Ma, L.; Chen, Q.; Ma, P.; Han, M. K.; Xu, Z.; Kang, Y.; Xiao, B.; Merlin, D. IRGD-Functionalized PEGylated Nanoparticles for Enhanced Colon Tumor Accumulation and Targeted Drug Delivery. Nanomedicine (Lond) 2017, 12 (16), 1991–2006. https://doi.org/10.2217/nnm-2017-0107.
(43) Zuo, H. iRGD: A Promising Peptide for Cancer Imaging and a Potential Therapeutic Agent for Various Cancers https://www.hindawi.com/journals/jo/2019/9367845/ (accessed 2020 -05 -11). https://doi.org/10.1155/2019/9367845.

(44) Kang, S.; Lee, S.; Park, S. IRGD Peptide as a Tumor-Penetrating Enhancer for Tumor-Targeted Drug Delivery. Polymers (Basel) 2020, 12 (9), 1906. https://doi.org/10.3390/polym12091906.
(45) Pullan, J. E.; Chemeiti, P.; Confeld, M.; Feng, L.; Froberg, J.; Choi, Y.; Mallik, S. Hypoxia Responsive Lipid Incorporation Into Bovine Milk Exosomes. Biomedical Science Instrumentation 2018, 54 (1), 293–300.
(46) Gamcsik, M. P.; Kasibhatla, M. S.; Teeter, S. D.; Colvin, O. M. Glutathione Levels in Human Tumors. Biomarkers 2012, 17 (8), 671–691. https://doi.org/10.3109/1354750X.2012.715672.
(47) Tu, Y.; Peng, F.; White, P. B.; Wilson, D. A. Redox-Sensitive Stomatocyte Nanomotors: Destruction and Drug Release in the Presence of Glutathione. Angewandte Chemie International Edition 2017, 56 (26), 7620–7624. https://doi.org/10.1002/anie.201703276.
(48) Pullan, J. E.; Confeld, M. I.; Osborn, J. K.; Kim, J.; Sarkar, K.; Mallik, S. Exosomes as Drug Carriers for Cancer Therapy. Mol. Pharmaceutics 2019, 16 (5), 1789–1798. https://doi.org/10.1021/acs.molpharmaceut.9b00104.
(49) Wijenayake, S.; Eisha, S.; Tawhidi, Z.; Pitino, M. A.; Steele, M. A.; Fleming, A. S.; McGowan, P. O. Comparison of Methods for Pre-Processing, Exosome Isolation, and RNA Extraction in Unpasteurized Bovine and Human Milk. PLoS One 2021, 16 (9), e0257633. https://doi.org/10.1371/journal.pone.0257633.
(50) Bansal, A.; Simon, M. C. Glutathione Metabolism in Cancer Progression and Treatment Resistance. J Cell Biol 2018, 217 (7), 2291–2298. https://doi.org/10.1083/jcb.201804161.
(51) Ding, N.; Zou, Z.; Sha, H.; Su, S.; Qian, H.; Meng, F.; Chen, F.; Du, S.; Zhou, S.; Chen, H.; Zhang, L.; Yang, J.; Wei, J.; Liu, B. IRGD Synergizes with PD-1 Knockout Immunotherapy by Enhancing Lymphocyte Infiltration in Gastric Cancer. Nat Commun 2019, 10. https://doi.org/10.1038/s41467-019-09296-6.
(52) Danhier, F.; Le Breton, A.; Préat, V. RGD-Based Strategies To Target Alpha(v) Beta(3) Integrin in Cancer Therapy and Diagnosis. Mol. Pharmaceutics 2012, 9 (11), 2961–2973. https://doi.org/10.1021/mp3002733.
(53) Liu, Z.; Wang, F.; Chen, X. Integrin Avβ3-Targeted Cancer Therapy. Drug Dev Res 2008, 69 (6), 329–339. https://doi.org/10.1002/ddr.20265.
(54) Sloan, E. K.; Pouliot, N.; Stanley, K. L.; Chia, J.; Moseley, J. M.; Hards, D. K.; Anderson, R. L. Tumor-Specific Expression of Avβ3 Integrin Promotes Spontaneous Metastasis of Breast Cancer to Bone. Breast Cancer Res 2006, 8 (2), R20. https://doi.org/10.1186/bcr1398.
(55) Alhalhooly, L.; Confeld, M. I.; Woo, S. O.; Mamnoon, B.; Jacobson, R.; Ghosh, S.; Kim, J.; Mallik, S.; Choi, Y. Single-Molecule Force Probing of RGD-Binding Integrins on Pancreatic Cancer Cells. ACS Appl. Mater. Interfaces 2022, 14 (6), 7671–7679. https://doi.org/10.1021/acsami.1c23361.
(56) Johnson-Arbor, K.; Dubey, R. Doxorubicin. In StatPearls; StatPearls Publishing: Treasure Island (FL), 2021.
(57) Calcagno, A. M.; Fostel, J. M.; To, K. K. W.; Salcido, C. D.; Martin, S. E.; Chewning, K. J.; Wu, C.-P.; Varticovski, L.; Bates, S. E.; Caplen, N. J.; Ambudkar, S. V. Single-Step Doxorubicin-Selected Cancer Cells Overexpress the ABCG2 Drug Transporter through Epigenetic Changes. Br J Cancer 2008, 98 (9), 1515–1524. https://doi.org/10.1038/sj.bjc.6604334.
(58) Zaidi, M.; Fu, F.; Cojocari, D.; McKee, T. D.; Wouters, B. G. Quantitative Visualization of Hypoxia and Proliferation Gradients Within Histological Tissue Sections. Front Bioeng Biotechnol 2019, 7. https://doi.org/10.3389/fbioe.2019.00397.
(59) Walsh, J. C.; Lebedev, A.; Aten, E.; Madsen, K.; Marciano, L.; Kolb, H. C. The Clinical Importance of Assessing Tumor Hypoxia: Relationship of Tumor Hypoxia to Prognosis and Therapeutic Opportunities. Antioxid Redox Signal 2014, 21 (10), 1516–1554. https://doi.org/10.1089/ars.2013.5378.
(60) Tassone, P.; Tagliaferri, P.; Perricelli, A.; Blotta, S.; Quaresima, B.; Martelli, M. L.; Goel, A.; Barbieri, V.; Costanzo, F.; Boland, C. R.; Venuta, S. BRCA1 Expression Modulates Chemosensitivity of BRCA1-Defective HCC1937 Human Breast Cancer Cells. Br J Cancer 2003, 88 (8), 1285–1291. https://doi.org/10.1038/sj.bjc.6600859.
(61) Toyoda, Y.; Takada, T.; Suzuki, H. Inhibitors of Human ABCG2: From Technical Background to Recent Updates With Clinical Implications. Front. Pharmacol. 2019, 10. https://doi.org/10.3389/fphar.2019.00208.
(62) Sarkadi, B.; Homolya, L.; Szakács, G.; Váradi, A. Human Multidrug Resistance ABCB and ABCG Transporters: Participation in a Chemoimmunity Defense System. Physiological Reviews 2006, 86 (4), 1179–1236. https://doi.org/10.1152/physrev.00037.2005.

TOC Graphic:

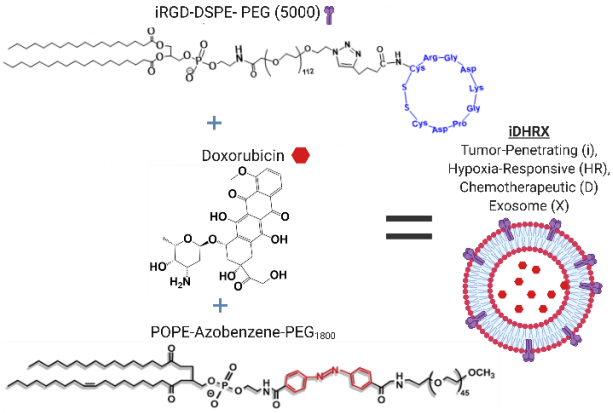
iRGD-DSPE- PEG (5000)
Doxorubicin
POPE-Azobenzene-PEG1800
iDHRX
Tumor-Penetrating (i),
Hypoxia-Responsive (HR),
Chemotherapeutic (D)
Exosome (X)